EUROPEAN COMMISSION
DIRECTORATE-GENERAL
Joint Research Centre

Institute for Environment and Sustainability

MODerate Resolution Imaging Spectroradiometer (MODIS)

JRC-FAPAR at 250 m resolution Algorithm Theoretical Basis Document

Nadine Gobron, Ophélie Aussedat and Bernard Pinty

European Commission -DG Joint Reseach Center,
Institute for Environment and Sustainability
Global Environmental Unit, TP 440
I–21020 Ispra (VA), Italy

July 2006 **JRC Publication No. EUR 22279 EN**

The mission of the Institute for Environment and Sustainability is to provide scientific and technical support to the European Union's policies for protecting the environment and the EU Strategy for Sustainable Development.

European Commission Directorate-General Joint Research Centre Institute for Environment and Sustainability http://ies.jrc.cec.eu.int http://www.jrc.cec.eu.int//

EUR 22279 EN Luxembourg: Office for Official Publications of the European Communities

Contents

List of Figures

List of Tables

1 Introduction

1.1 Purpose

This Algorithm Theoretical Basis document (ATBd) describes the Joint Research Centre (JRC) procedure used to retrieve information on the nature and properties of vegetated terrestrial surfaces from an analysis of the Top Of Atmosphere (TOA) data acquired **at 250 m spatial resolution** by the MODerate Resolution Imaging Spectroradiometer (MODIS), on board the Terra platform of National Aeronautics and Space Administration (NASA) (Salomonson et al. 1989).

The software takes the form of a set of several formulae which transform calibrated spectral directional reflectances into a single numerical value approximating the Fraction of Absorbed Photosynthetically Active Radiation (FAPAR) in the plant canopy. The methodology described in this document has been optimized to assess the presence on the ground of healthy live green vegetation. The optimization procedure has been constrained to provide an estimate of FAPAR in the plant canopy, although the outputs are expected to be used in a wide range of applications. This algorithm delivers, in addition to the FAPAR product, the so-called rectified reflectance values in the red and near-infrared spectral bands (MODIS Band 1 and Band 2). **The present procedure generates the rectified reflectance values at 250 m spatial resolution using MODIS data in the blue band at 500 m**. These rectified channels are virtual reflectances decontaminated at best from atmospheric and angular effects.

This document identifies the sources of input data, outlines the physical principles and mathematical background justifying the approach, describes the proposed algorithm, presents some results with actual data, and lists the assumptions and limitations of this technique.

1.2 Algorithm identification

The algorithm described below is called the 250-MODIS Vegetation Indicator (250-MOVI). It provides daily FAPAR products at 250 m of spatial resolution from MODIS. It follows from the MOVI algorithm described in Gobron et al. (2006) which is designed for MODIS data aquired at 500 m (*i.e.* MOD02HKM) and 1 km (*i.e.* MOD021KM), respectively.

1.3 Scope

This document outlines the algorithm which is recommended to generate FAPAR product and associated rectified red and near-infrared reflectance values at 250 m spatial resolution.

1.4 Revision history

This document presents the first release of JRC-FAPAR algorithm which is applicable to the MODIS data measured in the red and near-infared land bands at 250 m spatial resolution.

1.5 Other relevant documents

Other references to technical reports, ATBDs and additional information about MODIS can be found at the following internet address: `http://modis.gsfc.nasa.gov/`. A series of relevant reports and articles are included in the reference list appended to this document.

A time compositing procedure suitable for a number of surface applications requiring good geographical coverage is also described in Pinty et al. (2002).

2 Algorithm overview

2.1 Objectives of surface retrievals

The bulk of the solar radiation available to the Earth system is absorbed at or near the oceanic and continental surface. This energy is ultimately released to the atmosphere through the fluxes of infrared radiation, as well as sensible and latent heat. The phytosphere, which itself accounts for most of the biomass, affects these exchanges through a surface of contact (leaves) with the atmosphere estimated to be larger than the surface of the entire planet.

The state and evolution of terrestrial vegetation is characterized by a large number of physical, biochemical and physiological variables. Few of these are directly observable from space, but they jointly determine the Fraction of Absorbed Photosynthetically Active Radiation (FAPAR) which acts as an integrated indicator of the status and health of the plant canopy, and can reasonably be retrieved by remote sensing techniques. FAPAR plays a critical role in the biosphere path of the global carbon cycle and in the determination of the primary productivity of the land biosphere.

The state and evolution of the terrestrial vegetation cover thus concern a large number of users through such applications as agriculture, forestry, environmental monitoring, etc. Since plant canopies significantly affect the spectral and directional reflectance of solar radiation, it is expected that the analysis of repeated observations of these reflectances may lead to a better understanding of the fundamental processes controlling the biosphere, which, in turn, will support the definition of sustainable policies of environmental exploitation, and the control of the effectiveness of any adopted rules and regulations.

The overall scientific objective of the JRC-FAPAR algorithm is to exploit the spectral reflectance measurements acquired by solar instruments to provide users with reliable qualitative and quantitative information on the state of the plant cover over terrestrial areas. Specifically, the output value is meant to be easily interpreted in terms of FAPAR values.

The design of the 250-MOVI requires, in a first step, the estimate of the rectified reflectances at the red and near-infrared bands in order to minimize atmospheric and angular perturbations. The inputs are given by the MODIS land spectral bands in the red and near-infrared domains at a resolution of 250 meters (Band 1 and Band 2) and the blue spectral (Band 3) available at 500 meters. The rectification procedure of Band 1 and Band 2 in 250-MOVI uses information obtained from the rectification procedure, itself applied on those same spectral bands but at 500 m spatial resolution where the blue band (Band 3) is available; this standard rectification procedure is fully described in Gobron et al. (2006) and duplicated in this document for the sake of completeness.

These intermediary land surface products should prove useful for documenting the state of the land surfaces and also assessing the spatio-temporal variations in land cover type. Specifically, these rectified reflectances correspond to the amplitude parameter of the BRF entering the Rahman, Pinty, Verstraete (RPV) parametric model (Rahman et al. 1993). These are virtual, *i.e.*, not directly measurable in the field, spectral reflectances which are, at best, decontaminated from atmospheric and angular effects.

2.2 Instrument characteristics

The MODIS instrument is described in `http://modis.gsfc.nasa.gov/`. For the purpose of this document, it is sufficient to recall that MODIS is a solar instrument acquiring 36 spectral measurements between 0.4 μm to 14.4 μm. Two bands are imaged at a nominal resolution of 250 m at nadir, with five bands at 500 m, and the remaining 29 bands at 1 km. A 55-degree scanning pattern at the EOS orbit of 705 km achieves a 2,330-km swath and provides global coverage every one to two days. MODIS is not designed to acquire simultaneous measurements over any particular site under more than one geometry of illumination and observation, however, orbital constraints and instrumental specifications will inevitably result in different such geometries from pixel to pixel within a single image and for any given location between overpasses on consecutive days.

The proposed algorithm will thus focus on the exploitation of the spectral variability of the data, keeping in mind the possible perturbing effects that may result from variations in geometry within and between successive images.

2.3 Retrieval strategy

The specific objective of this document is to describe a spectral algorithm suitable to estimate FAPAR, optimized for the data acquired by the MODIS instrument at 250 m in the red and near-infrared spectral bands.

The strategy follows those already used for a series of optical instrument such as SeaWiFS (Gobron et al. 2002), VEGETATION (Gobron et al. 2002b), GLobal Imager (GLI) (Gobron et al. 2002a), MERIS (Gobron et al. 2004) and MODIS (Gobron et al. 2006).

The design criteria are:

1. to provide a high sensitivity to the Fraction of Absorbed Photosynthetically Active Radiation (FAPAR) when a vegetated area is detected,
2. to maintain a low sensitivity to soil and atmospheric conditions whenever vegetation is detected,
3. to exploit the multi-band specificity of the sensor,
4. to be independent of the geometry of illumination and observation,
5. to offer excellent discrimination capabilities, *i.e.*, the opportunity to distinguish various target types, and
6. **to be applied on data acquired in the red and near-infared bands at 250 m simultaneous with those acquired in the blue band at 500 m resolution**.

3 Algorithm description

3.1 Physics of the problem

The general theory behind the design of optimal spectral indices has been described in Verstraete and Pinty (1996), and its specific application to instruments has been addressed in Govaerts et al. (1999), Gobron et al. (1999) and Gobron et al. (2000).

The most recent implementation of the algorithm assumes that, 1) the FAPAR can be used to quantify the presence of vegetation and, 2) radiation transfer model simulations can be used to define appropriate scenarios over different representative land surfaces.

The bulk of the information on the presence of vegetation is contained *a priori* in the red and the near-infrared spectral bands, typically at wavelengths such as 620-670 nm and 841-876 nm, *i.e.* Band 1 and Band 2 of MODIS. Addressing the atmospheric problem consists in converting Top Of Atmosphere (TOA) Bidirectional Reflectance Factors (BRFs) into Top Of Canopy (TOC) BRFs.

Two classes of atmospheric radiative processes affect the measurements made by spaceborne satellites: absorption and scattering. Absorption of radiation by specific gases can be largely avoided by carefully choosing the spectral location of narrow bands. Further corrections can be implemented, if needed, by estimating the amount of these gases from other spectral bands. The effect of scattering cannot be avoided, and both molecular and aerosol scattering are strongly dependent on the wavelength of radiation. Hence, measurements in the blue region of the solar spectrum will provide values much more sensitive to atmospheric scattering than at longer wavelengths. In this approach, the characterization of plant canopies over fully or partially vegetated pixels currently relies on the analysis of data in 3 MODIS spectral bands, namely Band 3 at 459-479 nm, Band 1 at 620-670 nm, and Band 2 at 841-876 nm.

The spectral responses of these bands have been taken from the 6S code (see Vermote et al. (1997)). Figure 1 illustrates these theoretical values as function of the wavelength. A Look Up Table (LUT) of bidirectional reflectance factors representing the MODIS-like data has been created using the physically-based semi-discrete model of Gobron et al. (1997) to represent the spectral and directional reflectance of horizontally homogeneous plant canopies, as well as to compute the values of FAPAR in each of them. The soil data required to specify the lower boundary condition in this model were taken from Price (1995). The spectral values for the leaf reflectance and transmittance were simulated using the model from Jacquemoud and Baret (1990). The 6S atmospheric model of Vermote et al. (1997) has been used to represent the atmospheric absorption and scattering effects on the measured reflectances. The FAPAR values are computed using the closure of the energy balance inside the plant canopy in the spectral range 400 to 700 nm. The various geophysical scenarios performed to simulate the radiance fields are summarized in Table 1 and the geometrical conditions of illumination and observation are given in Table 2. The sampling of the vegetation parameters and angular values were chosen to cover a wide range of environmental conditions. These simulations constitute the basic information used to optimize the vegetation index. The sampling selected to generate the LUT has been chosen so as to generate a robust global vegetation index.

Once this LUT has been created, the design of the algorithm consists in defining the mathematical combination of spectral bands which will best account for the variations of the variable of interest (here, FAPAR) on the basis of (simulated) measurements, while

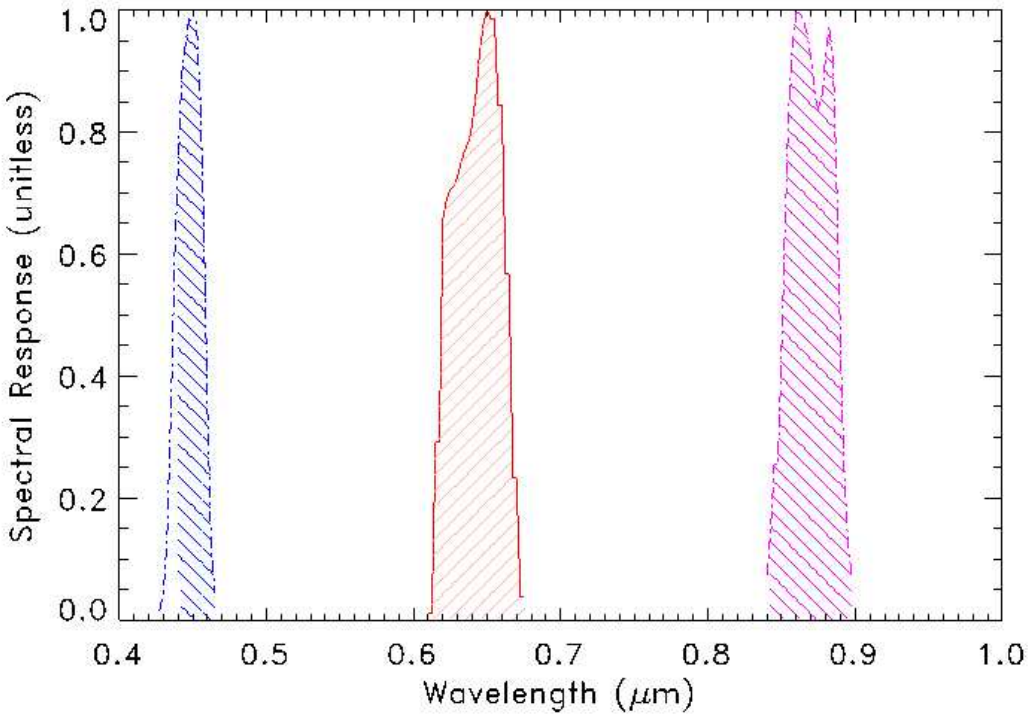

Figure 1: MODIS spectral responses of Band 1 (red color), 2 (pink color) and 3 (blue color) as a function of wavelength.

minimizing the effect of perturbing factors such as atmospheric or angular effects. This procedure is described in the next section.

3.2 Mathematical description of the algorithm

The proposed algorithm to compute the FAPAR value, is organized around three main consecutive steps.

1. As mentioned previously, because of the actual sampling strategy implemented by the MODIS instrument in the angular domain, it is not possible to retrieve the anisotropy of the radiance field. A parametric anisotropic function is implemented to account for variations in the signal due to changes in the geometrical conditions. The bidirectional reflectance model of Rahman et al. (1993) (RPV) is assumed to be appropriate for this task:

$$\rho_i(\theta_0, \theta_v, \phi) = \rho_{i0}\, F(\theta_0, \theta_v, \phi; k_i, \Theta_i^{hg}, \rho_{ic}) \tag{1}$$

where F characterizes the anisotropy of the medium in terms of three unknown parameters, namely k_i, Θ_i^{hg} and ρ_{ic} which depend exclusively on the intrinsic properties of the type of geophysical system for a given spectral band i. The function $F(\Omega; k_i, \Theta_i^{hg}, \rho_{ic})$ with $\Omega = (\theta_0, \theta_v, \phi)$ is given by:

$$F(\Omega; k_i, \Theta_i^{hg}, \rho_{ic}) = f_1(\theta_0, \theta_v, k_i)\, f_2(\Omega, \Theta_i^{hg})\, f_3(\Omega, \rho_{ic}) \tag{2}$$

Table 1: Geophysical scenarios used to simulate the radiance fields.

Medium	**Variable**	**Meaning**	**Range of values**
Atmosphere model (Vermote *et al.*, 1997)	τ_s	Aerosol opt. thickness	0.05, 0.3 and 0.8
Vegetation model (Gobron *et al.*, 1997)	LAI	Leaf Area Index	0, 0.5, 1, 2, 3, 4, and 5
	H_c	Height of Canopy	0.5 m and 2 m
	d_ℓ	Equivalent diameter of single leaf	0.01 m and 0.05 m
	LAD	Leaf Angle Distribution	Erectophile, Planophile
Soil data base (Price, 1995)	r_s	Soil reflectance	5 soil spectra, from dark to bright

Table 2: Illumination and observation geometries used to simulate the radiance fields.

Variable	**Angle**	**Values**
θ_0	Solar zenith angle	20° and 50°
θ_v	Sensor zenith angle	0°, 25°and 40°
ϕ	Sun-Sensor relative azimuth	0°, 90° and 180°

where

$$f_1(\theta_0, \theta_v, k_i) = \frac{(\cos\theta_0\ \cos\theta_v)^{k_i-1}}{(\cos\theta_0 + \cos\theta_v)^{1-k_i}} \tag{3}$$

$$f_2(\Omega, \Theta_i^{hg}) = \frac{1-\Theta_i^{hg\,2}}{\left(1+2\,\Theta_i^{hg}\ \cos g + \Theta_i^{hg\,2}\right)^{3/2}} \tag{4}$$

$$f_3(\Omega, \rho_{ic}) = 1 + \frac{1-\rho_{ic}}{1+G} \tag{5}$$

with

$$G = \left(\tan^2\theta_0 + \tan^2\theta_v - 2\ \tan\theta_0\ \tan\theta_v\ \cos\phi\right)^{1/2} \tag{6}$$

$$\cos g = \cos\theta_0\ \cos\theta_v + \sin\theta_0\ \sin\theta_v \cos\phi \tag{7}$$

The characterization of a geophysical system with the RPV model thus requires the estimation of four parameter values, namely ρ_{i0}, k_i, Θ_i^{hg} and, ρ_{ic} which are independent of the geometry of illumination and observation Ω.

The parameters intervening in function F are optimized separately in the three bands using the simulated BRFs emerging at the top of atmosphere.

2. The information contained in the band 3 (blue) is combined with that in the bands 1 and 2 (red and near-infrared) traditionally used to monitor vegetation, in order to generate "rectified bands" at these latter two wavelengths. The "rectification" is

done in such a way as to minimize the difference between those rectified bands and the spectral reflectances that would have been measured at the top of the canopy under identical geometrical conditions but in the absence of the atmosphere.

3. The FAPAR is then generated on the basis of these "rectified bands" at 500 m spatial resolution.

The proposed algorithm assumes that ratios of polynomials are appropriate to generate both the "rectified bands" with the following generic formula:

$$g_n(B_1, B_2) = \frac{l_{n,1}(B_1 + l_{n,2})^2 + l_{n,3}(B_2 + l_{n,4})^2 + l_{n,5}B_1B_2}{l_{n,6}(B_1 + l_{n,7})^2 + l_{n,8}(B_2 + l_{n,9})^2 + l_{n,10}B_1B_2 + l_{n,11}} \tag{8}$$

where B_1 and B_2 are the spectral bands at the appropriate step. The final formula itself is given by:

$$g_0(B_1, B_2) = \frac{l_{0,1}\, B_2 - l_{0,2}\, B_1 - l_{0,3}}{(l_{0,4} - B_1)^2 + (l_{0,5} - B_2)^2 + l_{0,6}} \tag{9}$$

$$\text{FAPAR} = g_0(\rho_{RBand1}, \rho_{RBand2}) \tag{10}$$

where ρ_{RBand1} and ρ_{RBand2} are the rectified reflectance values in the red and near-infrared bands described above. These, in turn, are estimated with

$$\rho_{R681}^{500m} = g_1(\tilde{\rho}_{Band3}^{500m}, \tilde{\rho}_{Band1}^{500m}) \tag{11}$$

$$\rho_{R865}^{500m} = g_2(\tilde{\rho}_{Band3}^{500m}, \tilde{\rho}_{Band2}^{500m}) \tag{12}$$

where

$$\tilde{\rho}_i^{500m} = \frac{\rho_i^{*500m}(\theta_0, \theta_v, \phi)}{F(\theta_0, \theta_v, \phi; k_i, \Theta_i^{hg}, \rho_{ic})} \tag{13}$$

and where all quantities X noted as X^{500m} correspond to reflectance values at 500 m resolution. ρ_i^{*500m} denotes the (simulated) top of atmosphere bidirectional reflectance factor in band i, while $\tilde{\rho}_i^{500m}$ is the bidirectional reflectance factor normalized by the anisotropic function F. An optimization procedure is applied to retrieve successively the optimal values of the coefficients intervening in the three steps mentioned above, namely k_i, Θ_i^{hg} and ρ_{ic}, and $l_{n,j}$ for the polynomials g_n, both for the rectified bands and for the final index itself.

1. In the first step, it is assumed that the anisotropic shapes of the BRFs simulated at the top of the atmosphere may change with the spectral wavelength of interest, but 1) do not depend on the geophysical systems specified to generate the BRFs and, 2) are independent of the spatial resolution of acquisition. Accordingly, for a given spectral band, the three parameters of the anisotropic function F are forced to be constant over the entire set of geophysical scenarios considered. In practice, this condition is achieved by minimizing the following cost functions:

$$\delta_i^2 = \sum_{\zeta,\Omega} \left[\left(\frac{\rho_i^*(\Omega)}{F(\Omega; k_i, \Theta_i^{hg}, \rho_{ic})} \right) - \tilde{\rho}_i \right]^2 \to 0 \tag{14}$$

where ζ represents the geophysical domain and Ω the angular domain over which the optimization is sought.

Since $\tilde{\rho}_i$ is assumed to be constant in the RPV model for each individual geophysical system taken separately, we can estimate the mean value of the BRFs over the Ω space for every geophysical system:

$$\frac{1}{N_{obs}} \sum_{\Omega} \rho_i^*(\Omega_j) = \frac{1}{N_{obs}} \sum_{\Omega} \tilde{\rho}_i \times F(\Omega_j; k_i, \Theta_i^{hg}, \rho_{ic}) \quad (15)$$

$$= \tilde{\rho}_i \frac{1}{N_{obs}} \sum_{\Omega} F(\Omega_j; k_i, \Theta_i^{hg}, \rho_{ic}) \quad (16)$$

where N_{obs} is the total number of angular situations. The model coefficient $\tilde{\rho}_i$ is thus approximated for each geophysical system as

$$\tilde{\rho}_i = \frac{1}{N_{obs}} \sum_{\Omega} \rho_i^*(\Omega_j) \Big/ \frac{1}{N_{obs}} \sum_{\Omega} F(\Omega_j; k_i, \Theta_i^{hg}, \rho_{ic}) \quad (17)$$

The cost function is rewritten as follows:

$$\delta_i^2 = \sum_{\zeta} \left[\frac{\rho_i^*(\Omega)}{F(\Omega; k_i, \Theta_i^{hg}, \rho_{ic})} \frac{1}{N_{obs}} \sum_{\Omega} F(\Omega_j; k_i, \Theta_i^{hg}, \rho_{ic}) - \frac{1}{N_{obs}} \sum_{\Omega} \rho_i^*(\Omega_j) \right]^2 \to 0 \quad (18)$$

2. To satisfy the various requirements described above, the optimization procedure is applied in the Band 1 and Band 2 separately, to derive the coefficients of g_1 and g_2. This is achieved by minimizing the following cost functions:

$$\delta_{g_i}^2 = \sum_{\zeta} \left[g_i(\tilde{\rho}_{Blue}, \tilde{\rho}_i) - \tilde{\rho}_i^{TOC} \right]^2 \to 0. \quad (19)$$

where

$$\tilde{\rho}_i^{TOC} = \frac{\rho_i^{TOC}(\Omega)}{F(\Omega, k_i^{TOC}, \Theta_i^{hg,TOC}, \rho_{ic}^{TOC})} \quad (20)$$

for which the anisotropic parameters, namely $k_i^{TOC}, \Theta_i^{hg,TOC}, \rho_{ic}^{TOC}$, were previously optimized at the top of canopy level.

3. Following the rectification of the BRFs in the previous step, the coefficients of g_0 are evaluated by minimizing the following cost function:

$$\delta_{g_0}^2 = \sum_{\zeta} \left[g_0(\rho_{RBand1}, \rho_{RBand2}) - \mathrm{FAPAR} \right]^2 \to 0. \quad (21)$$

In other words, the algorithm output is forced to take on values as close as possible to the FAPAR associated with the specified plant canopy scenarios. The simulated top-of-atmosphere spectral and directional reflectances generated by the coupled model have been exploited with an extended version of the FACOSI tool (Govaerts et al. 1999) to adjust the formulae on the basis of the given set of equations. The numerical results are summarized in Tables 3 to 6.

Figures 2 and 3 illustrate the impact of the "rectification" procedure, which combines simulated TOA reflectances in the blue band with simulated TOA reflectances in the red and NIR bands, respectively. The left panels on these figures show the relationships

Table 3: Values of the parameters for the anisotropic function F.

band	**Parameter values**		
	ρ_{ic}	k_i	Θ_i^{hg}
Blue (Band 3)	0.13704	0.56177	−0.03204
Red (Band 1)	−0.39924	0.70116	0.03376
NIR (Band 2)	0.63537	0.86830	−0.00081

Table 4: Coefficients for the polynomial g_1.

$l_{1,1}$	$l_{1,2}$	$l_{1,3}$	$l_{1,4}$	$l_{1,5}$	
−13.860	−0.018273	1.5824	0.081450	17.092	
$l_{1,6}$	$l_{1,7}$	$l_{1,8}$	$l_{1,9}$	$l_{1,10}$	$l_{1,11}$
0	0	0	0	0	1.0

Table 5: Coefficients for the polynomial g_2.

$l_{2,1}$	$l_{2,2}$	$l_{2,3}$	$l_{2,4}$	$l_{2,5}$	
−0.036557	−3.5399	8.3076	0.18702	−13.294	
$l_{2,6}$	$l_{2,7}$	$l_{2,8}$	$l_{2,9}$	$l_{2,10}$	$l_{2,11}$
0.77034	−4.9048	−2.3630	−2.6733	−37.297	0

Table 6: Coefficients for the polynomial g_0.

$l_{0,1}$	$l_{0,2}$	$l_{0,3}$	$l_{0,4}$	$l_{0,5}$	$l_{0,6}$
0.26130709	0.33489629	−0.00382980	−0.32136740	0.31415914	−0.010744180

between the spectral BRFs TOC normalized by the anisotropic function F, and BRFs TOA for all geophysical and angular scenarios described in Table 1. The scattering of the points is caused by changes in the atmospheric conditions and by the relative geometry of illumination and observation. The right panels show the effect of the "rectification" process, which reduces this dispersion. A perfect "rectification" would collapse all points on the 1:1 line for each of the surface types considered. It can be seen that this process is particularly efficient over dense vegetation, and that it reduces the systematic bias due to atmospheric effects on BRFs in both bands.

Figure 4 provides information on the performance of the algorithm in term of providing FAPAR values from the simulated BRF TOA values. The right panel shows the isolines of the 250-MOVI values in the spectral space of the rectified bands in the red (x-axis) and near-infrared (y-axis). It can be seen that the values varies between 0 and 1 over partially and fully vegetated surfaces and takes negative values out of the spectral domain of interest. The left panel of the same figure shows that 250-MOVI output is

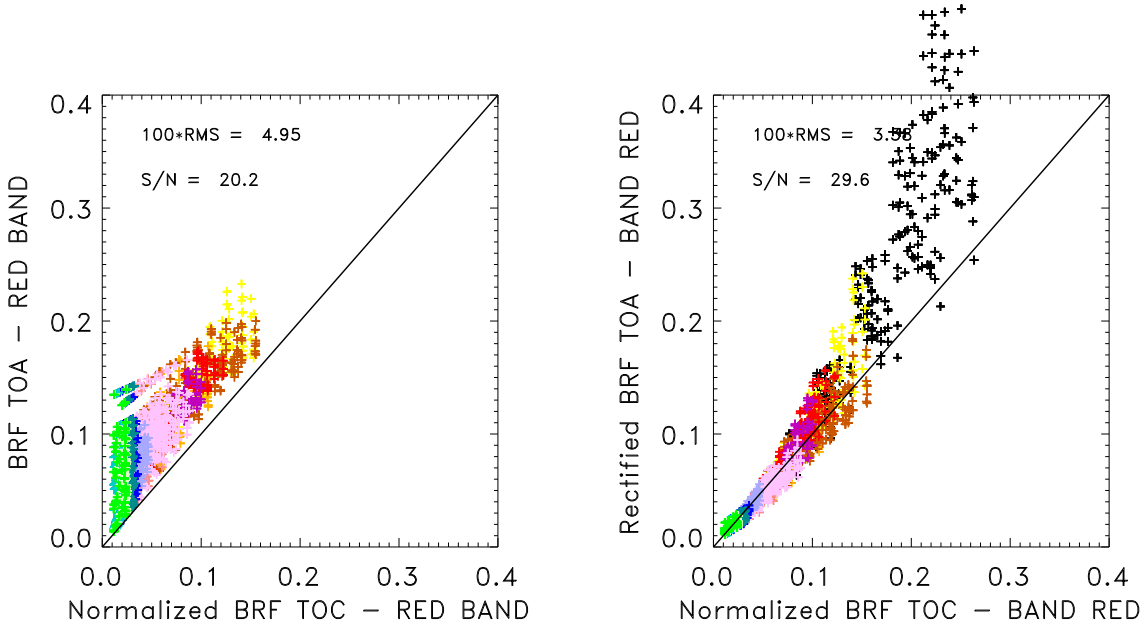

Figure 2: Left panel: relationship between the BRFs TOC normalized by the anisotropic function F, and BRFs TOA, for all conditions given in Table 1, in the red band. Right panel: relationship between the "rectified" reflectances and the corresponding BRFs TOC normalized by the anisotropic function F. The various colours represent different values of FAPAR for the plant canopies described in Table 1.

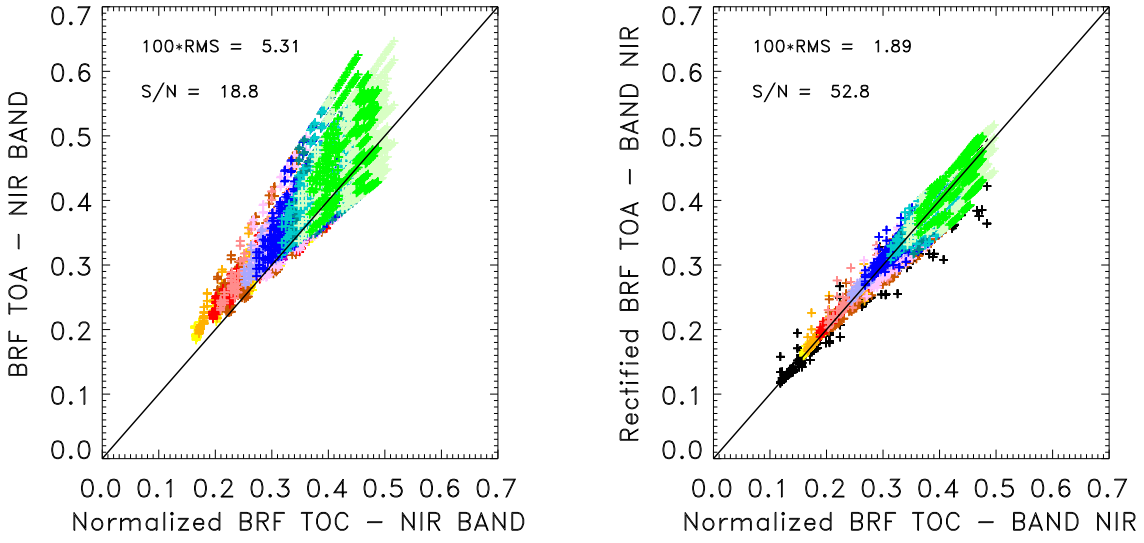

Figure 3: Same as Figure 2 except for the Band 2.

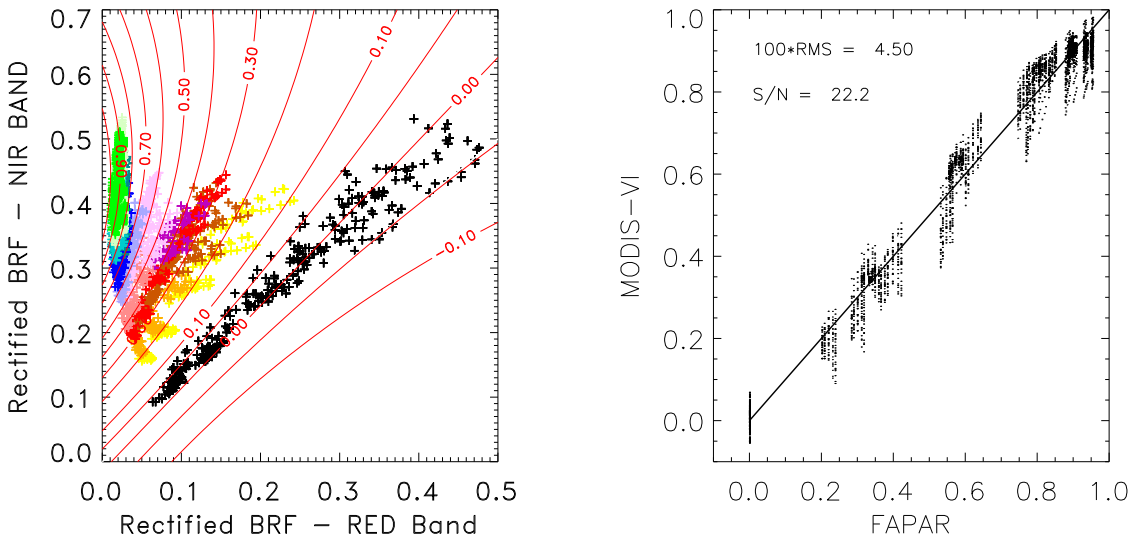

Figure 4: The right panel shows the isolines of 250-MOVI in the"rectified" spectral space together with the simulated radiances at the top of the atmosphere (see Table 1). The left panel shows the relationship between the index and the FAPAR values.

close to the FAPAR with a root mean square deviation closed to 0.045. Most of the remaining variability is probably caused by the various conditions that were considered in the geophysical scenarios (see Table 1). In fact, this variability results from conflicting requirements on the insensitivity of the algorithm to soil, atmospheric and geometrical effects in the MODIS land spectral bands.

3.3 Error budget estimates

Since the algorithm has been optimized to provide a high sensitivity to FAPAR, a measurable biophysical variable, its capacity to detect the presence of green vegetation can be objectively assessed. For the particular geophysical scenarios in Table 1 and angular sampling given in Table 2, the root mean square deviation value of the fit between these two quantities is at about 0.045. Following the method proposed by Leprieur et al. (1994), the performance can be evaluated with the help of a signal to noise ratio. In the present case, it was found that the signal to noise ratio of the algorithm is equal to **22.2**.

4 Implementation for the 250 m MODIS red and near-infrared bands combined with 500 m MODIS blue band.

The description given in the previous section is common to both MOVI (Gobron et al. 2006) and 250-MOVI algorithms. This section describes the procedure suggested to operate the 250-MOVI algorithm with actual MODIS data (MOD02QKM).

In order to perform the rectification step on 250 m pixels in the band red and near-infrared, respectively, we will assume that the relationship between the TOA reflectances and the associated rectified channels, for each spectral band, does not depend on the

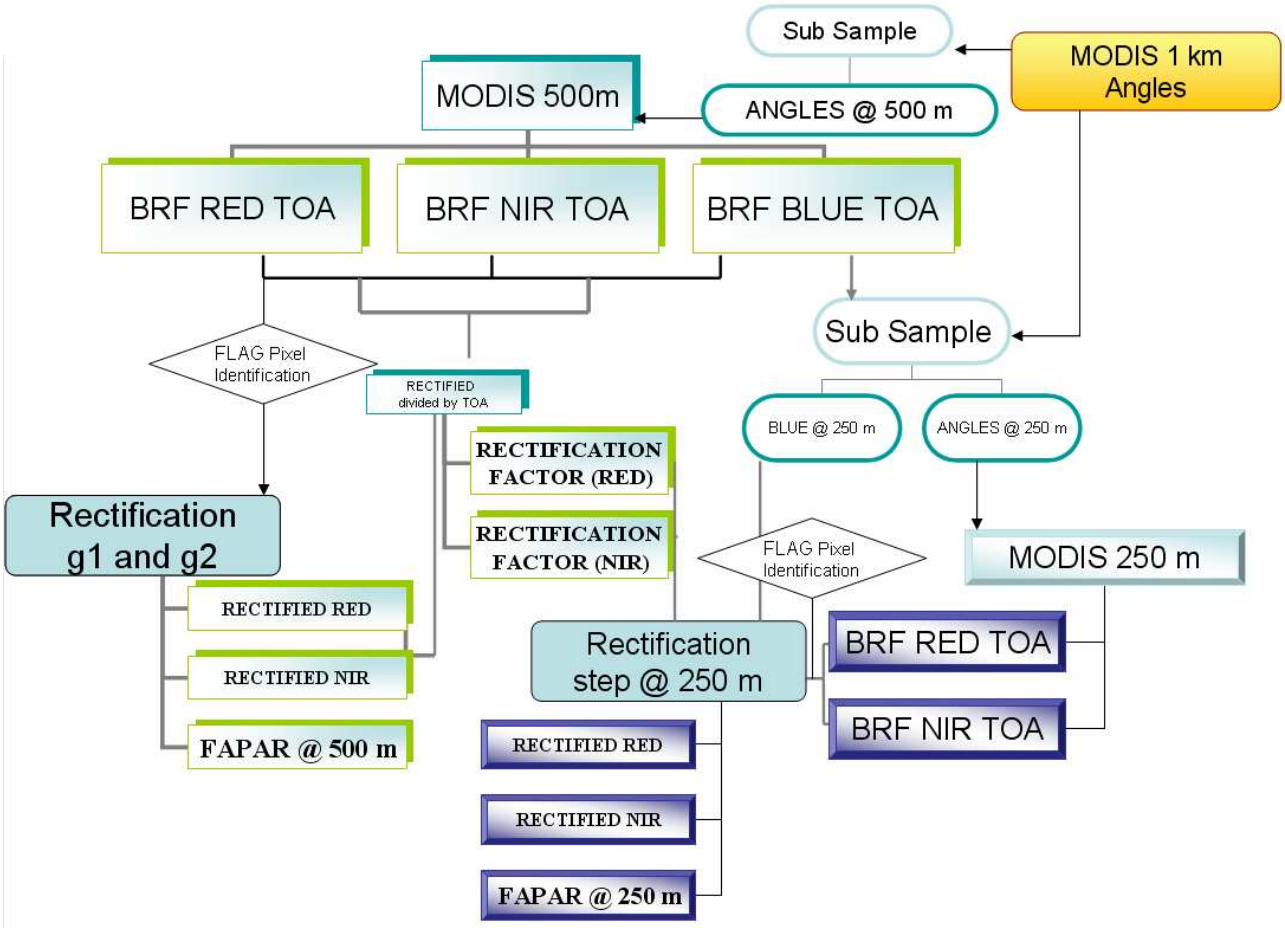

Figure 5: Flow chart of the JRC-FAPAR algorithm at 250 m

spatial resolution of the input data. The rectification procedure can thus be operated with 500 m pixel resolution which allows us to estimate two spectral "rectification factors", namely f_{R681} and f_{R865}, computed using Eqs. (22) and (23):

$$f_{R681} = \frac{\rho_{R681}^{500m}}{\rho_{Band1}^{*500m}} \tag{22}$$

$$f_{R865} = \frac{\rho_{R865}^{500m}}{\rho_{Band2}^{*500m}} \tag{23}$$

where ρ_{R681}^{500m} and ρ_{R865}^{500m} are the rectified channels using data at 500 m in the red and near-infrared band, respectively, and ρ_{Band1}^{*500m} and ρ_{Band2}^{*500m} are the corresponding TOA data in Band 1 and Band 2 at 500 m, respectively. Note, that we assume here that the anisotropy funtion, F, does not depend on the spatial resolution of the input data.

Figure 5 shows the flow chart of the proposed processing to estimate the rectification factors, f_{R681} and f_{R865}, which are required to further generate the FAPAR product at 250 m resolution from MODIS data. For all pratical proposes, these factors are sub-sampled at 250 m, that is, a single value of f_λ is assigned over 4 pixels at 250 m for Band 1 and Band 2 associated with the closest single pixel at 500 m for Band 3. The sub-sample is

done using a nearest-neigbor technique in the following section.

The rectified channels at 250 m are thus computed using Eqs (24) and (25):

$$\rho_{R681}^{250m} = f_{R681} \times \rho_{Band1}^{*250m} \quad (24)$$
$$\rho_{R865}^{250m} = f_{R865} \times \rho_{Band2}^{*250m} \quad (25)$$

Finally, the FAPAR is calculated with Eq. (10) at the resolution of 250 m using the rectified red and near-infrared channels at 250 m, that is:

$$FAPAR^{250m} = g_0(\rho_{R681}^{250m}, \rho_{R865}^{250m}) \quad (26)$$

5 Applications

In order to evaluate the proposed rectification scheme, we propose in this section to apply and compare the both rectification schemes using MODIS data at 500 m. In this exercice, various rectification factors, f, are computed at a number of low spatial resolution (from 2 km to 50 km) data generated by an aggregation of the original 500 m data.
Figure 6 (7) shows the comparisons (scatter-plots and histograms of differences) between the rectified channels in the red (near-infrared) band which have been computed with the rectification factors estimated from the data at lower spatial resolution (y-axis) as a function of these same rectified channels derived from the 500 m resolution only (x-axis). Figure 8 illustrates the impact on the procedure on the FAPAR products when decreasing the spatial resolution for the rectification factors. This spatial resolution varies successively from 2 km, 3 km, 4 km, 10 km and 50 km from the top left panel to the bottom right panel, respectively. This exercise has been performed with MODIS data acquired on June 1, 2003 at location surrounding the Harvard forest [41.54°N 43.54°N 83.17°W 81.17°W].

Each panel in these three figures reports the averaged value of the differences, which varies from 0.0006 (−0.0002) to 0.005 (0.0087) in the red (near-infrared) from 2 km up to 50 km. The corresponding standard deviation of differences, σ, is also computed and takes value from 0.0074 (0.0054) to 0.0118 (0.0184). The correlation coefficient goes from 0.9539 (0.9946) to 0.8593 (0.9305). These statistics suggest that the proposed rectification step can be reasonably applied at spatial resolutions higher than a couple of kms. The impact of this rectification on FAPAR is such that the averaged values of differences, the associated standard deviations and correlation coefficients vary from 0.0026, 0.037, 0.9837 to 0.0045, 0.0496, 0.9699, respectively. As can be logically expected, the performances of the procedure degrades with the spatial resolution (Fig. 6, 7, 8 from top left to bottom rigth panels): the closest the spatial resolution of the channels are, the better the FAPAR results will be.

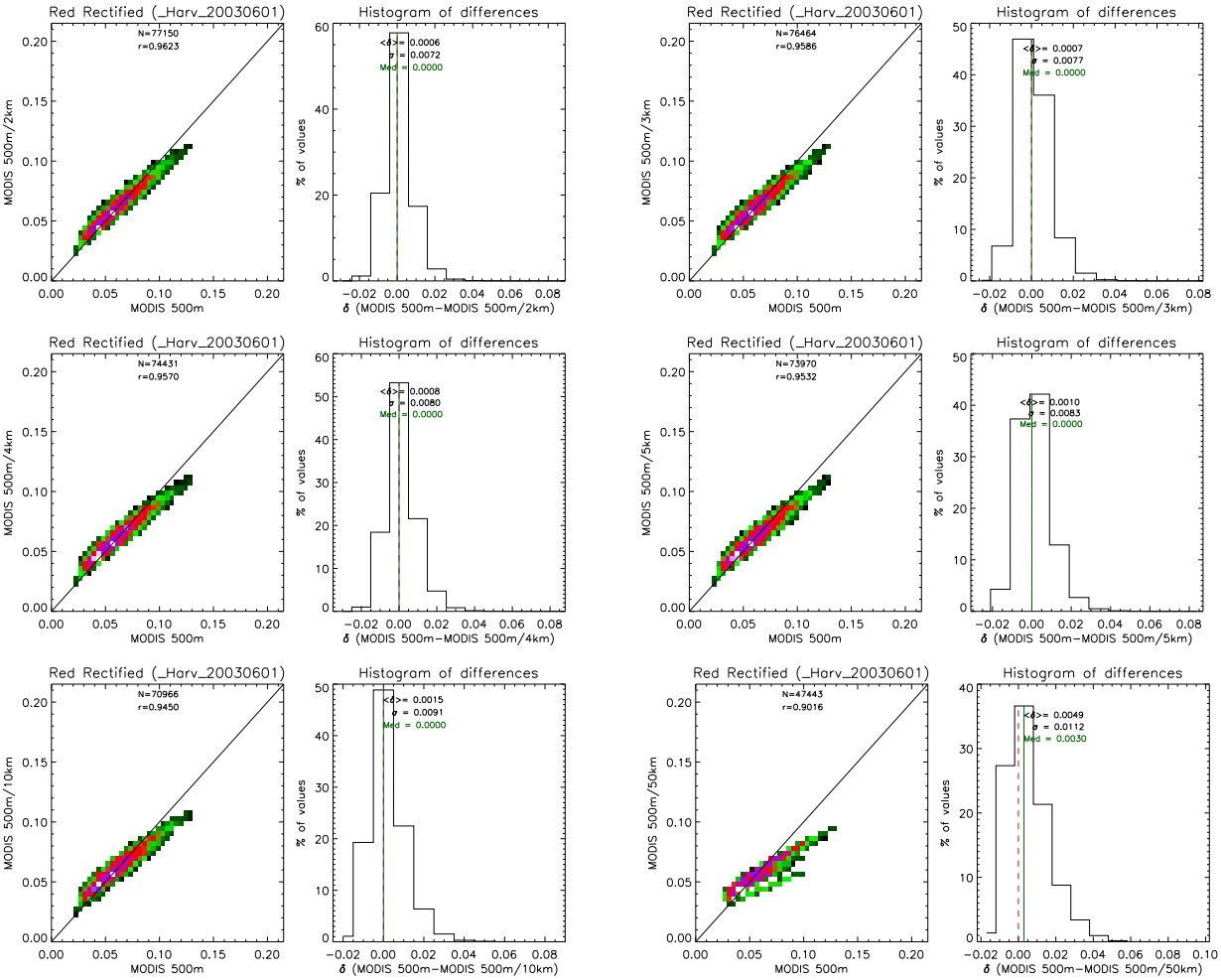

Figure 6: Scatter-plots and histograms of differences between the rectified channel when using the rectification factors computed with aggregated data at 2, 3, 4, 5, 10 and 50 km (y-axis) and the standard rectification computed with data at 500 m only (x-axis) in the red band.

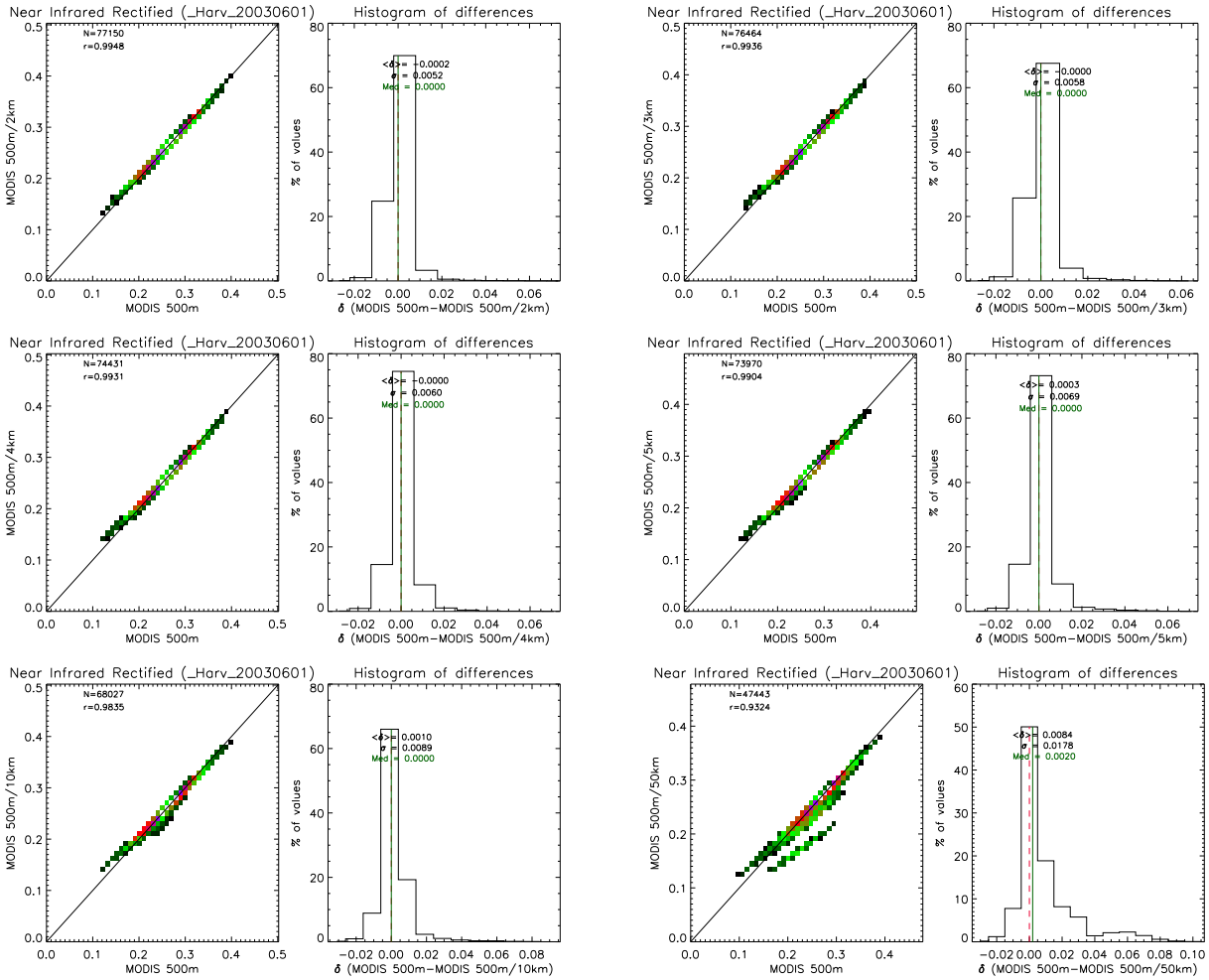

Figure 7: Scatter-plots and histograms of differences between the rectified channel when using the rectification factors computed with aggregated data at 2, 3, 4, 5, 10 and 50 km (y-axis) and the standard rectification computed with data at 500 m only (x-axis) in the near-infrared band.

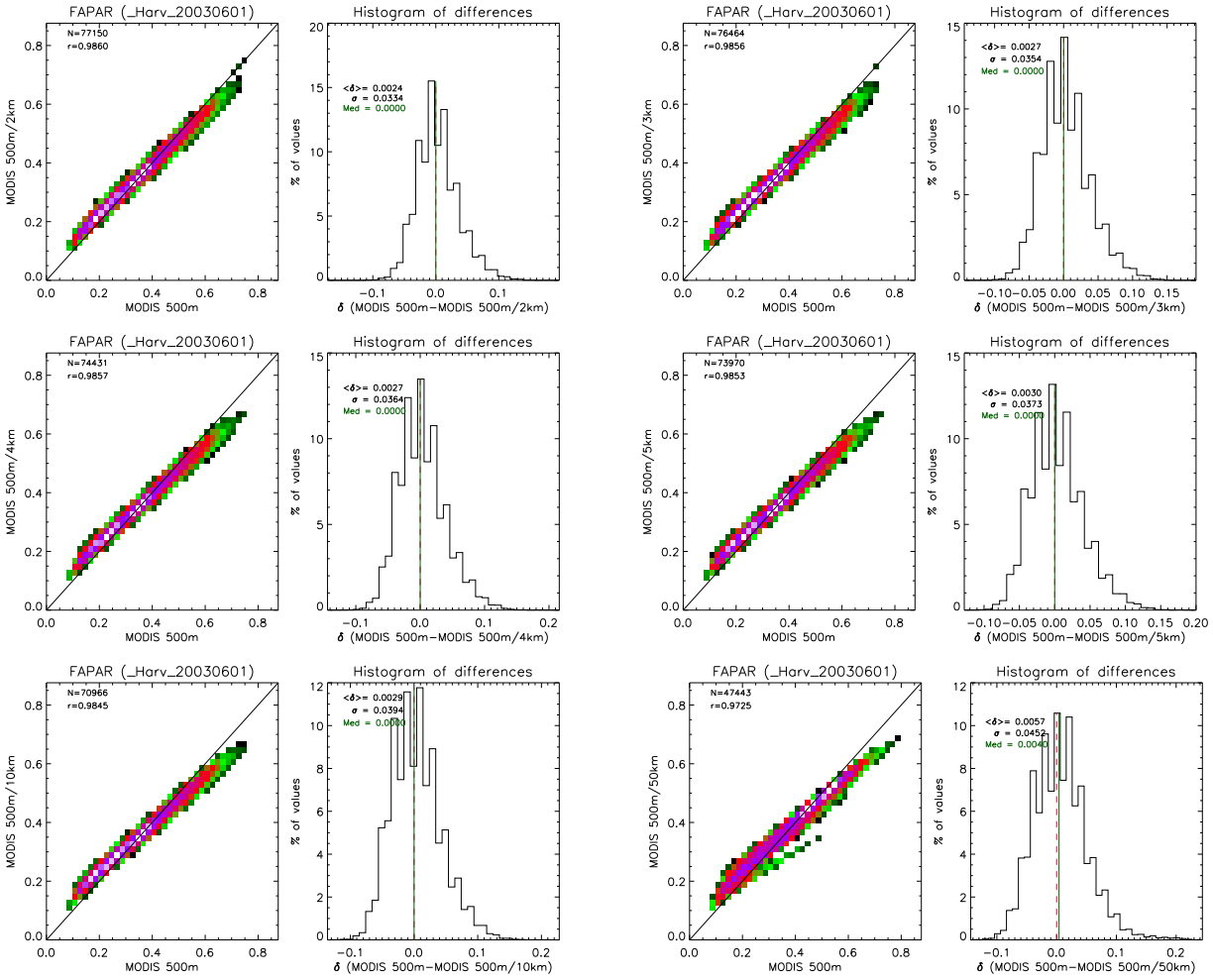

Figure 8: Scatter-plots and histograms of differences between the FAPAR values when using the rectification factors computed with aggregated data at 2, 3, 4, 5, 10 and 50 km (y-axis) and the standard rectification computed with data at 500 m only (x-axis).

The three images displayed in Figure 9 correspond to FAPAR products derived from MODIS data acquired around the Harvard site for which ground-estimates of FAPAR are available for year 2002 (Turner et al. 2005). The map on the left hand side panel shows the FAPAR value computed at 250 m, whereas the two other maps on the right hand side correspond to FAPAR value derived at 500 m: the top image uses rectification factors from 1 km resolution data and the bottom image uses the standard rectification procedure, *i.e.* similar to products generated by the MOVI algorithm.

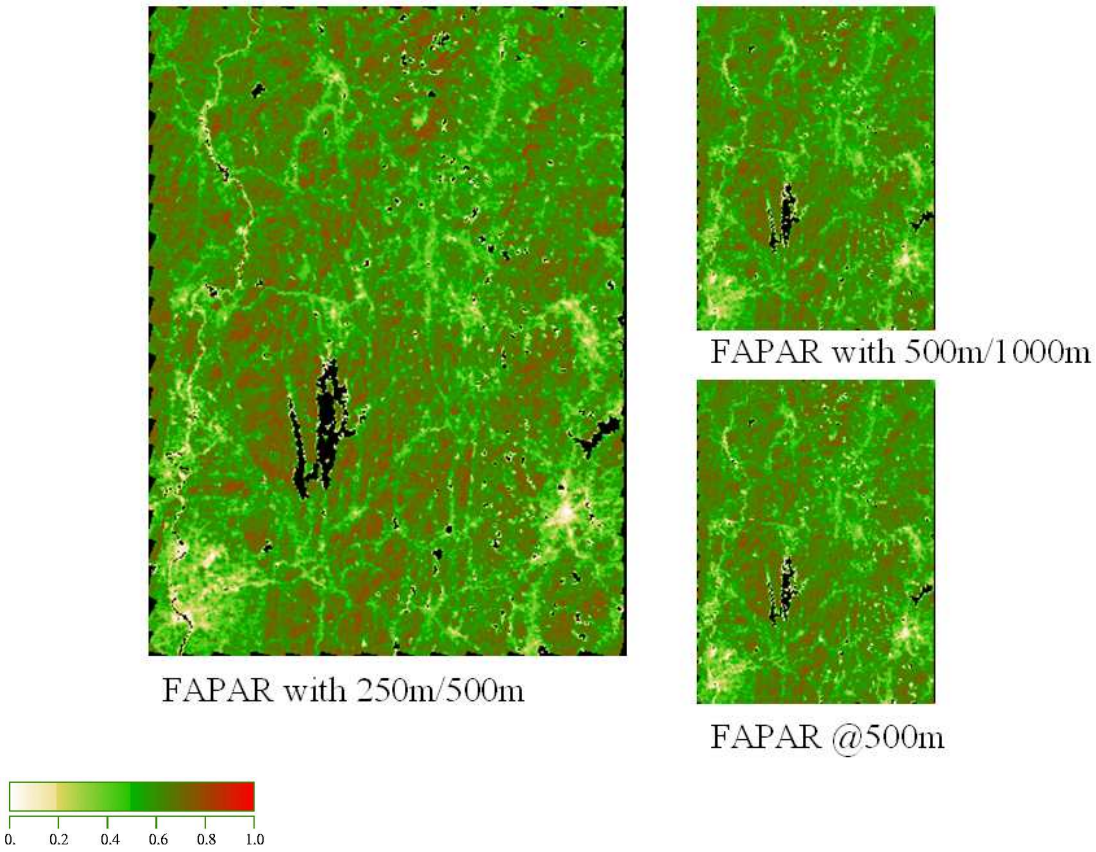

Figure 9: Daily FAPAR maps over the region of Harvard [41.54°N 43.54°N 83.17°W 81.17°W] using MODIS data acquired on the 6 of September 2002 at 250 m (left hand side) and at 500 m (right hand side). The map on the bottom panel corresponds to the results obtained using the original JRC-FAPAR algorithm at 500 m whereas the two others have been processed using lower resolution data for estimating the rectification factors.

The FAPAR comparison results corresponding to the maps displayed in Figure 9 are plotted on the top panel in Figure 10. The correlation coefficient, when comparing the two methods, takes a value of 0.9899, the averaged value of the difference is about -0.0007 and the standard deviation is equal to 0.0263. The bottom panels of this figure correspond to the comparison results of FAPAR products over the same region but using data acquired on June 1, 2003 in order to sample different type of angular and atmospheric conditions over that same land surface. This result illustrates that some deviation of the FAPAR values can be expected although the averaged value of differences, equal to 0.002 in this case, remains significantly less than the anticipated accuracy on the daily FAPAR

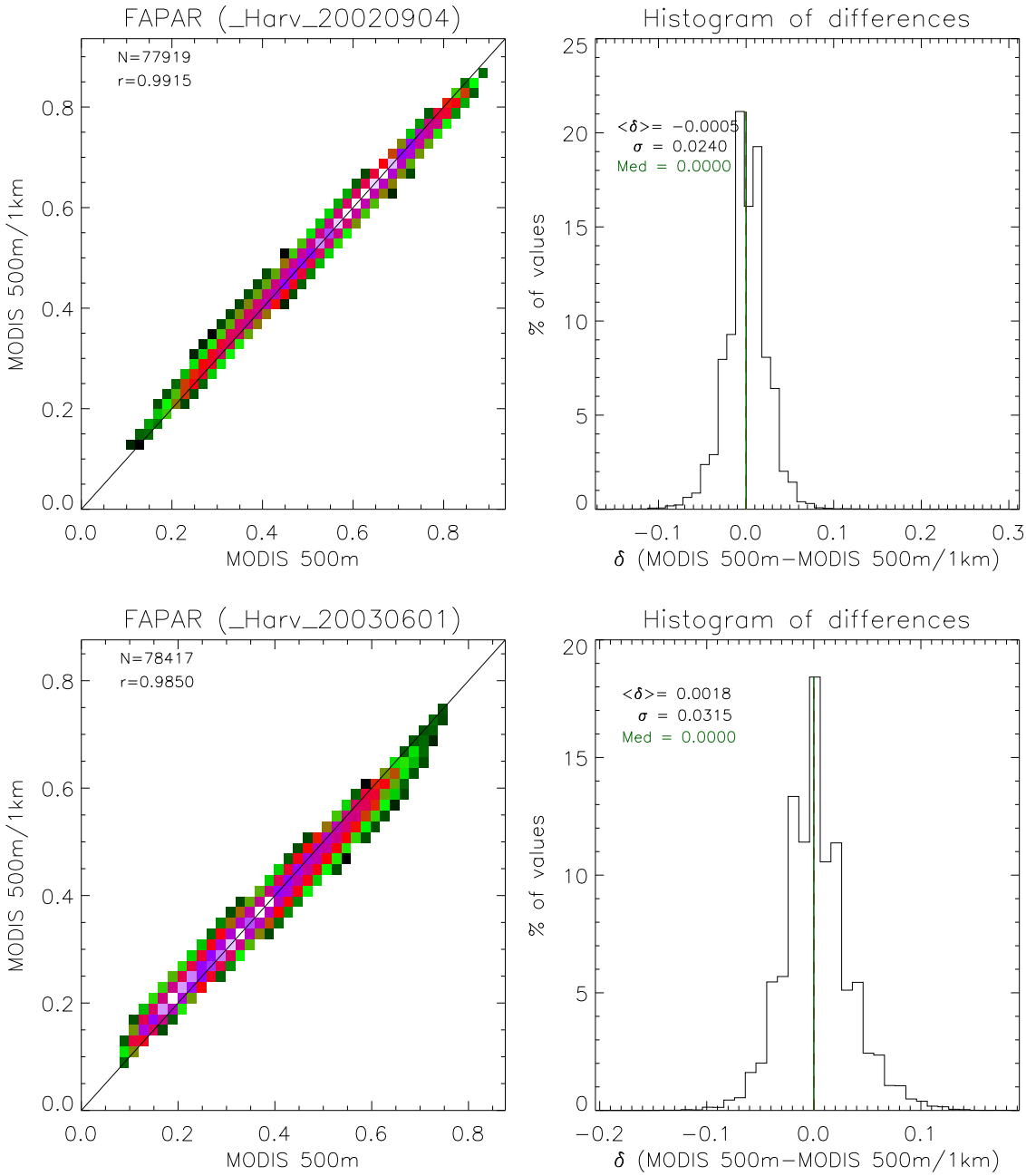

Figure 10: Scatter-plots and histograms of differences of daily FAPAR products over the region of Harvard [41.54°N 43.54°N 83.17°W 81.17°W] using MODIS data acquired at 500 m on the September 6, 2002 (top panel) and June 1, 2003 (bottom panel).

products.

To further evaluate the performances of the 250-MOVI algorithm, the latter has been applied with MODIS data acquired over the Harvard forest site during year 2002. The time series of the FAPAR products using data at 500 m are shown on the top panel in Figure 11. On this figure, the dark blue dotted points correspond to the output delivered by the standard MOVI algorithm and the light blue dotted points correspond to the output delivered by 250-MOVI, that is after generating the rectification factors at 1 km (after aggregation of the 500 m).

The bottom panel of Figure 11 shows FAPAR values generated over the Harvard forest site using actual MODIS data at 1 km (red color), 500 m (dark blue color) and 250 m (orange color) available for year 2002. These FAPAR values have been produced by the algorithm relevant to each spatial resolution. The error bars indicate the standard deviations over 2 (4) $\times$ 2 (4) pixels around the central pixel location. Note that, at a few dates, the 250-MOVI algorithm could not deliver results due to the identification of clouds/cloud shadows or any other events generating a flagged value at 250 m spatial resolution (see Section 5.1.1).

The differences between all these time series of FAPAR products remain small along the season and, for all practical purposes, statistically undiscernible from the pre-specified FAPAR accuracy of ± 0.1. The same remark applies when comparing these remote sensing against the corresponding ground-based estimates (approximated from in-situ measurements of the leaf area index (Turner et al. 2005)) for the first seven months of the year. As discussed in Gobron et al. 2006, the enhanced discrepancy appearing during the senescence phase (about one month lag) may be a consequence of using total (in the ground-based estimates) instead of green (in the retrieval algorithm) leaf area index when assessing the FAPAR value.

This exercice indicates that the 250-MOVI algorithm is able to generate FAPAR products on a routine basis using actual MODIS data available at the highest spatial resolution. This should prove useful for a number of local to regional applications requiring the analysis of high spatial resolution information like agricultural monitoring. The coupling of the 250-MOVI and MOVI algorithms offers a range of applications for instance for the analysis of multiscale processes.

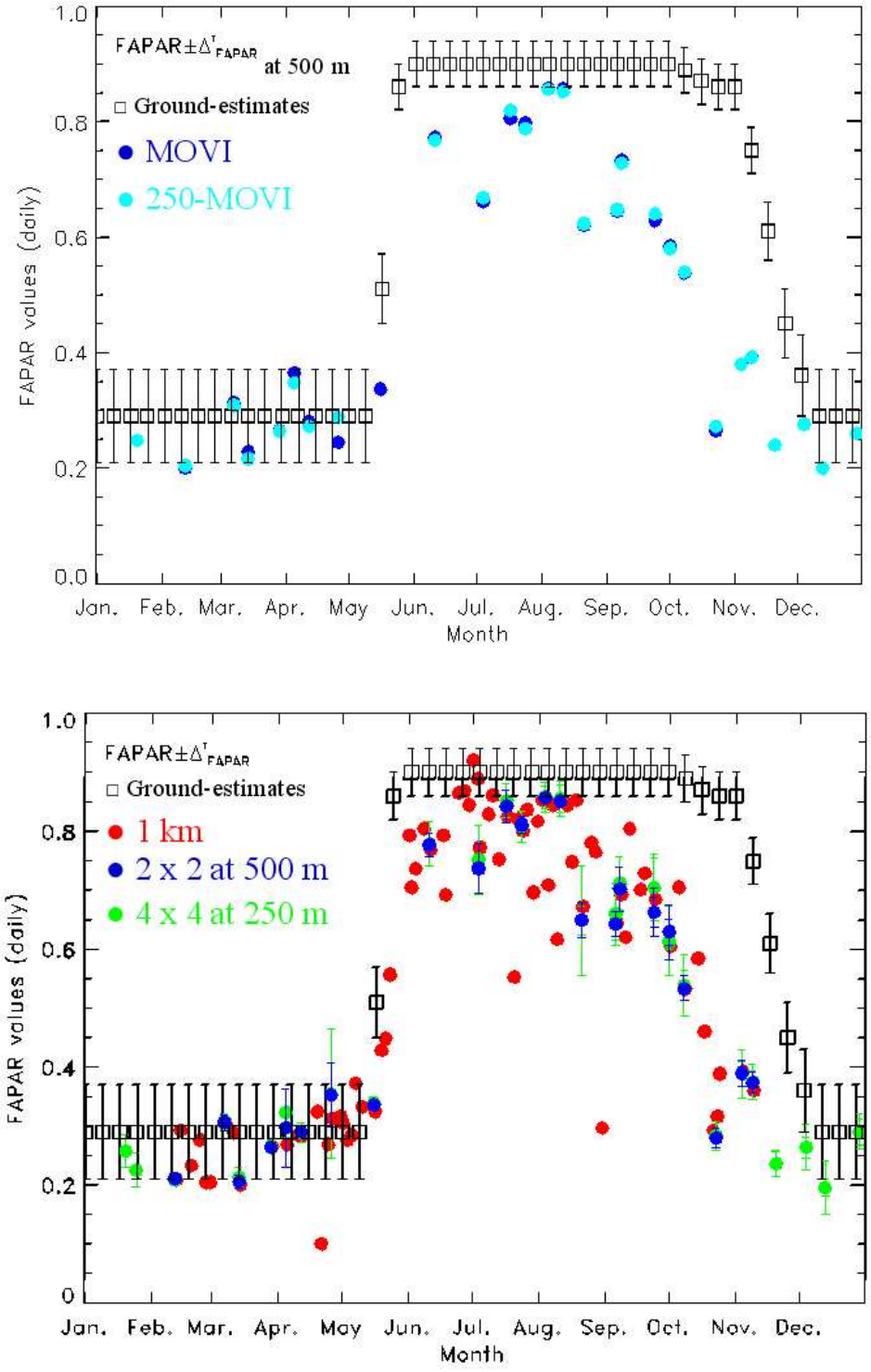

Figure 11: Top Panel: Time series of FAPAR over Harvard forest using MODIS data at 500 m. The dark blue dotted points correspond to the output delivered by the standard MOVI algorithm and the light blue dotted points correspond to the output delivered by 250-MOVI, that is after generating the rectification factors at 1 km (after aggregation of the 500 m). Bottom panel: Time series of FAPAR over Harvard forest using MODIS data at 1 km (red color), 500 m (dark blue color) and 250 m (green color) during year 2002. The error bars indicate the standard deviations over 2 (4) $\times$ 2 (4) pixels around the central pixel location. The ground-based estimates are derived from the measurements of leaf area index and are represented by the squares symbols.

5.1 Practical considerations

5.1.1 Quality control and diagnostics

A simple approach is proposed to associate a label to each pixel of the MODIS data in order to optimize the various steps of the processing to be achieved over land surfaces. Table 7 indicates the tests applied and the associated categories for discriminating the major geophysical systems (also identified with an identification number), namely clouds, bright surfaces, vegetated surfaces, cloud shadow or and water bodies. In the data product, the various identification numbers correspond to a set of flag values.
As can be seen from Table 7, the pixel labeling is performed on the basis of an ensemble of thresholds using only the values in the spectral bands used in the algorithm. For each geophysical category, the ensemble of tests has been established on the basis of knowledge of the multi-spectral signatures of the geophysical systems. The proposed approach classifies the vast majority of the pixels without requiring any other ancillary information. A more sophisticated labeling scheme could not be reasonably considered given the processing constraints imposed by the computing resources.

It is strongly recommended to apply the spectral flag algorithm at both 500 m and 250 m, separately, in order to use the rectification factors for the red and near-infrared bands at 250 m and the blue band sub-sampled at 250 m, respectively.

5.1.2 Output

The output generated by this algorithm consists in one FAPAR value, one value for the rectified red and near-infrared, at the highest resolution, respectively. The output field also contains the description of the geometry of illumination and observation, and one flag value for each pixel in the data input stream.

The flag value corresponds to the identification (ID) numbers described in section 5.1.1. If the ID value is equal to 0, the value of FAPAR is considered valid and the physical range of values lies in between 0 and 1.0.

If the ID number is equal either to 1 (“bad data”), 2 (“cloud, snow and ice”) or 3 (“water body and deep shadow”), the value of FAPAR has not been computed and the reported value is equal to its error value.

If the ID number is equal to 4 (“bright surface”), the value has been set at 0.

If ID number is equal to 5 (“undefined”), the value has not been computed and the reported value is set to its error value.

If the ID number is equal to 6, the value was less than 0 and the reported value is equal to 0.

If the ID number is equal to 7, the value was larger than 1 and the reported value is reset to 1.

6 Assumptions and limitations

6.1 Assumptions

The following assumptions have been made in the design of the 250-MODIS JRC-FAPAR algorithm:

Table 7: Pixel labeling criteria

Identification number (ID)	**Spectral tests**	**Associated categories**
0	$0 < \rho_{BLUE} < 0.277138$ and $0 < \rho_{RED} < 0.470685$ and $0 < \rho_{NIR} < 0.713182$ and $0 < \rho_{BLUE} \leq \rho_{NIR}$ and $\rho_{NIR} \geq 1.35\,\rho_{RED}$	vegetated surface
1	$\rho_{BLUE} \leq 0$ or $\rho_{RED} \leq 0$ or $\rho_{NIR} \leq 0$	bad data
2	$\rho_{BLUE} \geq 0.277138$ or $\rho_{RED} \geq 0.470685$ or $\rho_{NIR} \geq 0.713182$	cloud, snow and ice
3	$0 < \rho_{BLUE} < 0.277138$ and $0 < \rho_{RED} < 0.470685$ and $0 < \rho_{NIR} < 0.713182$ and $\rho_{BLUE} > \rho_{865}$	water body and deep shadow
4	$0 < \rho_{BLUE} < 0.277138$ and $0 < \rho_{RED} < 0.470685$ and $0 < \rho_{NIR} < 0.713182$ and $0 < \rho_{BLUE} \leq \rho_{NIR}$ and $1.35\,\rho_{RED} > \rho_{NIR}$	bright surface
5	$\rho_{R_{RED}} < 0$ or $\rho_{R_{NIR}} < 0$	undefined
6	$250 - MOVI < 0$	no vegetation
7	$250 - MOVI > 1$	vegetation (out of bounds)

1. The spectral reflectances used as input to this algorithm have to be corrected for the seasonally variable distance between the Earth and the Sun.

2. The plane-parallel approximation for radiation transfer has been assumed to be valid in the atmosphere.

3. Plant canopies are assumed to be horizontally homogeneous within the MODIS 250 m and 500 m pixel.

4. All orographic effects have been ignored.

5. Adjacency effects have been ignored.

6.2 Limitations

The following limitations apply to the algorithm described in this version of the document:

1. The retrieval of vegetation characteristics in hilly or mountainous regions may or may not be reliable. If the approach turns out to be unreliable in the presence of significant topographical features, additional tests may have to be implemented to screen out these regions on the basis of appropriate Digital Elevation Model (DEM) data. This would imply access to the corresponding elevation data sets, to reliably navigated MODIS data, and the presence of an additional orographic flag.

2. The optimization of the algorithm was performed using a set of simulated TOA reflectance values which are expected to represent the most commonly encountered geophysical conditions. Although a wide range of possibilities were investigated, there is no guarantee that the most common geophysical scenarios have been implemented.

3. The sun zenith angle should be lower than 60 degrees (due to the limitation of the radiative transfer models.)

4. The viewing zenith angle should be smaller than 50 degrees.

7 Algorithm requirements

The implementation of the proposed 250-MOVI algorithm to estimate FAPAR requires three different types of information, namely, the input data from the MODIS sensor (at 250 m (MOD02QKM) and 500 m (MOD02HKM) as well as the values of the solar and viewing zenith and azimuth angles at 1 km (from either the MOD021KM or MOD03 products)), a set of ancillary data and a set of mathematical functions. The ancillary data are the set of coefficients given in Tables 3 to 6. The mathematical functions are given by equations (2), (8), (9), (13), (23) to (26).

The input data are the BRFs measured by the instrument at blue, red and near-infrared bands, together with the geometrical conditions of illumination and observation, namely θ_0, θ_v, ϕ. The sun-sensor relative azimuth, ϕ, is limited to the range [0°, 180°] and the backscatter/hot spot (forwardscatter/specular) direction is defined at 0° (180°).

References

Gobron, N., O. Aussedat, and P. Bernard (2006). Moderate Resolution Imaging Spectroradiometer, JRC-FAPAR Algorithm Theoretical Basis Document. EUR Report No. 22164 EN, Institute for Environment and Sustainability.

Gobron, N., O. Aussedat, B. Pinty, M. Taberner, and M. M. Verstraete (2004). Medium Resolution Imaging Spectrometer (MERIS) - Level 2 Land Surface Products - Algorithm Theoretical Basis Document-Revision 3.0. EUR Report No. 21387 EN, Institute for Environment and Sustainability.

Gobron, N., B. Pinty, O. Aussedat, J. M. Chen, W. B. Cohen, R. Fensholt, V. Gond, K. F. Huemmrich, T. Lavergne, F. Mélin, J. L. Privette, I. Sandholt, M. Taberner, D. P. Turner, M. Verstraete, and J.-L. Widlowski (2006). Evaluation of FAPAR Products for Different Canopy Radiation Transfer Regimes: Methodology and Results using JRC Products Derived from SeaWiFS against ground-based estimations. *Journal of Geophysical Research 10.1029/2005JD006511*.

Gobron, N., B. Pinty, F. Mélin, M. Taberner, and M. M. Verstraete (2002). Sea Wide Field-of-View Sensor (SeaWiFS) - An optimized FAPAR algorithm - Theoretical Basis Document. EUR Report No. 20148 EN, Institute for Environment and Sustainability.

Gobron, N., B. Pinty, M. M. Verstraete, and Y. Govaerts (1997). A semi-discrete model for the scattering of light by vegetation. *Journal of Geophysical Research 102*, 9431–9446.

Gobron, N., B. Pinty, M. M. Verstraete, and Y. Govaerts (1999). The MERIS Global Vegetation Index (MGVI): description and preliminary application. *International Journal of Remote Sensing 20*, 1917–1927.

Gobron, N., B. Pinty, M. M. Verstraete, and M. Taberner (2002a). Global Land Imager (GLI) - An optimized FAPAR algorithm - Theoretical Basis Document. EUR Report No. 20147 EN, Institute for Environment and Sustainability.

Gobron, N., B. Pinty, M. M. Verstraete, and M. Taberner (2002b). VEGETATION - An optimized FAPAR algorithm - Theoretical Basis Document. EUR Report No. 20146 EN, Institute for Environment and Sustainability.

Gobron, N., B. Pinty, M. M. Verstraete, and J.-L. Widlowski (2000). Advanced spectral algorithm and new vegetation indices optimized for up coming sensors: Development, accuracy and applications. *IEEE Transactions on Geoscience and Remote Sensing 38*, 2489–2505.

Govaerts, Y., M. M. Verstraete, B. Pinty, and N. Gobron (1999). Designing optimal spectral indices: a feasibility and proof of concept study. *International Journal of Remote Sensing 20*, 1853–1873.

Jacquemoud, S. and F. Baret (1990). PROSPECT: A model of leaf optical properties spectra. *Remote Sensing of Environment 34*, 75–91.

Leprieur, C., M. M. Verstraete, and B. Pinty (1994). Evaluation of the performance of various vegetation indices to retrieve vegetation cover from AVHRR data. *Remote Sensing Reviews 10*, 265–284.

Pinty, B., N. Gobron, F. Mélin, and M. M. Verstraete (2002). A Time Composite Algorithm Theoretical Basis Document. EUR Report No. 20150 EN, Joint Research Centre, Institute for Environment and Sustainability.

Price, J. C. (1995). Examples of high resolution visible to near-infrared reflectance spectra and a standardized collection for remote sensing studies. *International Journal of Remote Sensing 16*, 993–1000.

Rahman, H., B. Pinty, and M. M. Verstraete (1993). Coupled surface-atmosphere reflectance (CSAR) model. 2. Semiempirical surface model usable with NOAA Advanced Very High Resolution Radiometer data. *Journal of Geophysical Research 98*, 20,791–20,801.

Salomonson, V. V., W. L. Barnes, P. W. Maymon, M. H. E., and H. Ostrow (1989). MODIS: Advanced facility instrument for studies of the earth as a system. *IEEE Transactions on Geoscience and Remote Sensing 27(2)*, 145–153.

Turner, D. P., W. D. Ritts, W. B. Cohen, T. Maeirsperger, S. T. Gower, A. Kirschbaum, S. W. Running, M. Zhao, S. Wofsy, B. Dunn, A. Law, J. Campbell, W. Oechel, H. J. Kwon, T. Meyers, E. Small, S. Kurc, and J. Gamon (2005). Site-level evaluation of satellite-based global terrestrial gross primary production and net primary production monitoring. *Global Change Biology 11*, 666–684.

Vermote, E., D. Tanré, J. L. Deuzé, M. Herman, and J. J. Morcrette (1997). Second simulation of the satellite signal in the solar spectrum: An overview. *IEEE Trans. Geoscience Remote Sensing 35-3*, 675–686.

Verstraete, M. M. and B. Pinty (1996). Designing optimal spectral indices for remote sensing applications. *IEEE Transactions on Geoscience and Remote Sensing 34*, 1254–1265.

8 Acknowledgements

The MODIS data used in this study were acquired as part of the NASA's Earth-Sun System Division and archived and distributed by the Goddard Earth Sciences (GES) Data and Information Services Center (DISC) Distributed Active Center (DAAC). The authors thank the BigFoot project, specially Waren B. Cohen and David P. Turner, for the avaibility of the ground-base estimates of FAPAR over Harvard site.

The mission of the JRC is to provide customer-driven scientific and technical support for the conception, development, implementation and monitoring of EU policies. As a service of the European Commission, the JRC functions as a reference centre of science and technology for the Union. Close to the policy-making process, it serves the common interest of the Member States, while being independent of special interests, whether private or national.